PAPER

Remarkable static and dynamic NLO response of alkali and superalkali doped macrocyclic [hexa-]thiophene complexes; a DFT approach†

Hasnain Sajid, [ID] [a] Faizan Ullah, [ID] [a] Sidra Khan,[a] Khurshid Ayub, [ID] [a] Muhammad Arshad[b] and Tariq Mahmood [ID] *[a]

In this study, the nonlinear optical (NLO) response of alkali metal atom (Li, Na and K) and their corresponding superalkali (Li_3O, Na_3O and K_3O) doped six membered cyclic thiophene (6CT) has been explored. The optimized geometries of complexes; Li@6CT, Na@6CT, K@6CT, Li_3O@6CT, Na_3O@6CT and K_3O@6CT depict that the superalkalis and alkali metals interact through the active cavity of 6CT. Interaction energies reveal that superalkalis have higher interaction with 6CT than alkali metals. The nonlinear optical (NLO) response of the reported complexes is estimated *via* both static and dynamic hyperpolarizabilities which are further rationalized by the HOMO−LUMO gap, natural bond orbital (NBO) charge transfer, dipole moment, polarizabilities and β_{vec}. A remarkably high NLO response is computed for Na_3O@6CT among all of the complexes. The static hyperpolarizability of the Na_3O@6CT complex is 5×10^4 au along with the highest β_{vec} value (2.5×10^4 au). High charge transfer ($1.53e^-$) and small E_{H-L} gap (2.96 eV) is responsible for such a large NLO response. For dynamic NLO responses, electro-optic Pockel's effect (EOPE) and second-harmonic generation (SHG) are explored. A very large quadratic nonlinear optical response (3.8×10^{-12} au) is observed for the Na_3O@6CT complex. Moreover, the absorption spectrum of the Na_3O@6CT complex shows ultra-high transparency in the ultraviolet and visible regions unlike any other of its counterparts.

1 Introduction

To date, significant consideration has been devoted to the fabrication of high performance nonlinear optical (NLO) materials,[1–4] due to their utility in electro-optic devices.[5–7] To fulfil this demand, various kinds of novel NLO materials with excess electrons have been designed.[8,9] It is very well documented that the excess electrons play a pivotal role in the large NLO response.[10,11] Excess electrons can be generated by capping a material with alkali metal atoms.[12] Thus alkali metal doping leads to large first and second hyperpolarizabilities of the systems.[13,14] Munsif *et al.*,[15] reported the exceptionally high NLO response of inorganic nanocages upon doping with alkali metal atoms. In their study, the authors claimed that the hyperpolarizability of potassium doped boron phosphide (inorganic nanocage) was the highest (7.9×10^5 au) ever reported. Maria and co-workers illustrated the exceptional increase in the hyperpolarizability of inorganic systems to 1.3×10^4 au from 0.00 au (pure material) upon doping with potassium metal.[16] In

another similar report, Maria *et al.*,[17] studied the nonlinear optical behaviour of inorganic nanocages. Their results suggested the hyperpolarizability of such systems was greatly enhanced upon capping with alkali metal atoms. Like inorganic systems, the NLO behaviour of organic systems is equally enhanced on complexation with alkali metals. For example, Li *et al.*,[8] theoretically designed a novel electride by adsorbing lithium metal on calix[4]pyrrole. The resulting electride molecule showed a large hyperpolarizability value (7326 au) which was twenty times larger than that of isolated calix[4]pyrrole systems. Based on the above discussion, it can be concluded that the doping of alkali metals remarkably enhance the opto-electronic properties of inorganic as well as organic systems.

In the recent decades, superalkalis, a kind of superatom clusters are attaining more interest as compared to alkali metal atoms. The superalkalis have greater affinity of donating valance electrons due to the lower vertical ionization potential.[18] Therefore, their usage in nonlinear optics advocated significant interest of experimental and theoretical researchers. It has been observed that the superalkalis doping increases the hyperpolarizability of the inorganic materials such as aluminium phosphide,[19] boron phosphide[20] and silicon carbide nanocages.[21] Apart from the inorganic systems, the NLO response of organic materials doped with superalkalis is also investigated. The organic molecules are expected to have giant NLO response because of their extended π-

[a]*Department of Chemistry, COMSATS University Islamabad, Abbottabad Campus, Abbottabad-22060, Pakistan. E-mail: mahmood@cuiatd.edu.pk*

[b]*Institute of Chemistry, University of the Punjab, Lahore, Pakistan*

conjugation.[22–24] In this regard, the nonlinear behaviour of graphdiyne was measured upon doping with superalkalis. Shehzadi et al.,[25] reported the dramatic increase in the first hyperpolarizability of superalkalis doped graphdiyne to 7.7×10^4 au. In another similar report, the remarkable enhancement in the NLO response of graphdiyne sheet upon complexation with superalkalis is demonstrated by Kosar et al.[26] The authors compared the NLO response of M_3O and M_3S (M = Li, Na & K) complexed graphdiyne and observed that both showed equal effect. In our previous report, we have presented that superalkalis (M_3O) doping in cyclic oligofuran remarkably enhances the NLO response. We reported that the cyclic conjugated ring systems can effectively be used as high NLO material due to their electron dense active cavity.[27]

The area of alkali and superalkalis doped cyclic thiophene ring system needs to be further explored. Thus, here we intend to compare the NLO response of macrocyclic hexathiophene ring (6CT) upon complexation with alkali metal atom (Li, Na, K) and their superalkalis analogues (Li_3O, Na_3O and K_3O). The geometric, electronic and nonlinear optical properties of alkali and superalkalis doped 6CT i.e., Li@6CT, Na@6CT, K@6CT, Li_3O@6CT, Na_3O@6CT and K_3O@6CT complexes are studied computationally. The NLO behaviour of said complexes are investigated via first hyperpolarizability (β_o), electro-optical Pockels effect (EOPE), second harmonic generation (SHG), and nonlinear refractive index (n_2) calculations.

2 Computational methods

Geometry optimizations of complexes are performed with two high level Minnesota functionals including M05-2X and M06-2X along with 6-31G(d,p), 6-31+G(d,p) and 6-311+G(d,p) basis sets. All calculations are performed with Gaussian09 software.[28] The interaction energies of complexes are defined by the expression below (eqn (1)).

$$E_{int} = E_{complex} - E_{6CT} - E_{SA/AA} \qquad (1)$$

where $E_{complex}$, E_{6CT} and $E_{SA/AA}$ are the energies of alkali atoms/superalkalis@6CT complex, cyclic hexathiophene and superalkalis/alkali atoms, respectively. Frontier molecular orbital (FMO) and NBO analysis are performed for the estimation of HOMO–LUMO (H–L) gap and amount of charge transfer of 6CT, respectively, upon complexation with alkali/superalkalis. To confirm the charge transfer and variation of H–L gaps, density of state (DOS) spectra are plotted through GaussSum software.[29] The polarizability, first hyperpolarizability calculations are benchmarked at M05-2X, M06-2X and LC-BLYP functionals with 6-31+G(d,p) basis set. However, the dynamic NLO responses of complexes are calculated at LC-BLYP because it is reported as a best functional for the estimation of nonlinear optical properties due to the full range separation with 1.00 correct fraction of nonlocal exchange functional.[15,30] The polarizability (α_o), first hyperpolarizability (β_o) and second order hyperpolarizability β_{vec} are defined as:

$$\alpha_o = \frac{1}{3}\left(\alpha_{xx} + \alpha_{yy} + \alpha_{zz}\right) \qquad (2)$$

$$\beta_o = (\beta x^2 + \beta y^2 + \beta z^2)^{1/2} \qquad (3)$$

$$\beta_{vec} = \sum_i \frac{\mu_i \beta_i}{|\mu|} \qquad (4)$$

where $\beta_x = \beta_{xxx} + \beta_{xyy} + \beta_{xzz}$, $\beta_y = \beta_{yyy} + \beta_{xzz} + \beta_{yxx}$, $\beta_z = \beta_{zzz} + \beta_{zxx} + \beta_{zyy}$

$$\beta_i = \sum(\beta_{ijj} + \beta_{jji} + \beta_{jij})i, j = \{x, y, z\} \qquad (5)$$

The second hyperpolarizability (γ_o) is estimated as:

$$\gamma_o = \sqrt{\gamma_x{}^2 + \gamma_y{}^2 + \gamma_z{}^2}$$

The frequency dependent NLO response in terms of the second harmonic generation (SHG) $\beta(-2\omega, \omega, \omega)$, the electro-optical Pockels effect (EOPE) $\beta(-\omega, \omega, 0)$, electro-optic Kerr effect (EOKE) form $\gamma(-\omega, \omega, 0, 0)$ and SHG form $\gamma(-2\omega, \omega, \omega, 0)$ are estimated at two standard Nd:Yag laser frequencies: $\omega = 0.0428$ au (1064 nm) and $\omega = 0.0856$ au (532 nm).

The frequency dependent/dynamic NLO response is computed through Coupled Perturbed Kohn–Sham (CPKS) method[31] and results are analyzed through Multiwfn software.[32] The dynamic first hyperpolarizability can be represented using the following equation:

$$\beta(\omega) = [\beta_x{}^2(\omega) + \beta_y{}^2(\omega) + \beta_z{}^2(\omega)]^{1/2}$$

where the coefficients of second harmonic generation (SHG) are obtained using

$$\beta_i = \beta_{iii}(-2\omega, \omega, \omega) + \beta_{ijj}(-2\omega, \omega, \omega) + \beta_{ikk}(-2\omega, \omega, \omega)$$

And the coefficients of electro-optical Pockels effect (EOPE) are obtained from

$$\beta_i = \beta_{iii}(-\omega, \omega, 0) + \beta_{ijj}(-\omega, \omega, 0) + \beta_{ikk}(-\omega, \omega, 0).$$

3 Results and discussion

3.1 Optimized geometries and stabilities

The six membered cyclic thiophene ring (6CT) is doped with three alkali metal atoms (Li, Na, K) and superalkalis (Li_3O, Na_3O and K_3O) to form AA@6CT (alkali metal doped) and SA@6CT (superalkalis doped) complexes. The different orientations of interactions are possible due to the various sensitive positions of 6CT. All these orientations are studies and their geometries are given in ESI (Fig. S1–S3).† Among all possibilities, the most stable geometries are considered for detailed analysis and their structures are displayed in Fig. 1. The interaction energies of AA@6CT and SA@6CT complexes are calculated at two Minnesota functionals i.e., M05-2X & M06-2X. The selection here is based on the previous reports, revealing the higher accuracy of Minnesota functionals to estimate the noncovalent interactions. For even better analysis, calculations are performed by using 6-31G (d,p), 6-31+G(d,p) and 6-311+G(d,p) basis sets. The interaction energies of complexes are listed in Table 1. Broadly,

the interaction energies of SA@6CT complexes are higher at all methods as compared to AA@6CT complexes which might be due to the higher electron density on superalkalis than alkali atom. Among all the complexes, the highest interaction energies are computed for Li_3O@6CT complex at M05-2X functional. The interaction energies of Li_3O@6CT complex are −76.60,
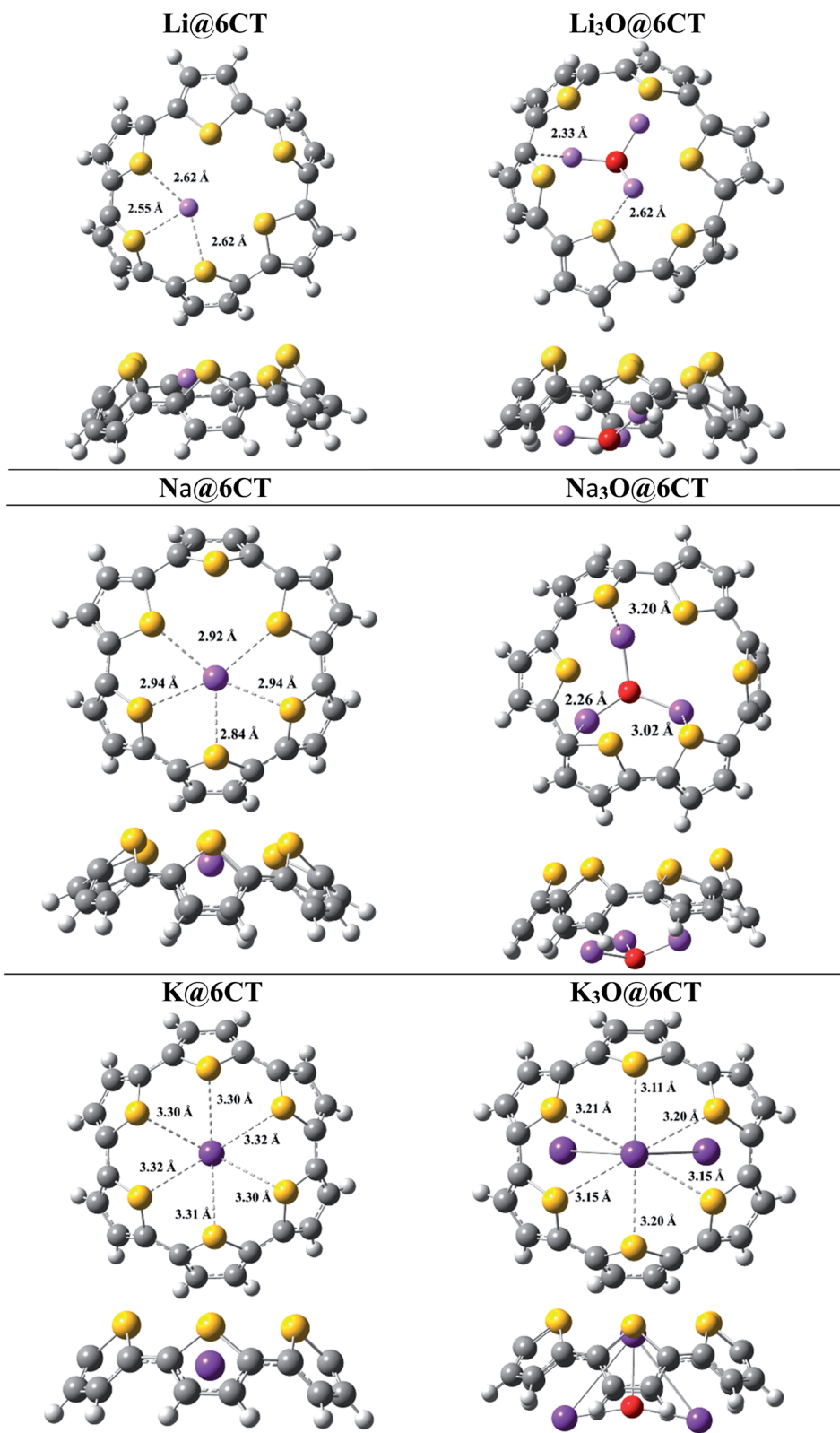

Fig. 1 Top and side view of most stable optimized geometries of AA@6CT and SA@6CT complexes.

Table 1 Benchmark interaction energies (in kcal mol^{-1}) of SA@6CT and AA@6CT complexes at different level of density functional theory

Complexes	M052X			M062X		
	6-31G (d,p)	6-31+G (d,p)	6-311+G (d,p)	6-31G (d,p)	6-31+G (d,p)	6-311+G (d,p)
Li@6CT	−41.07	−40.29	−41.90	−39.54	−38.85	−40.44
Li$_3$O@6CT	−76.60	−71.86	−70.34	−72.76	−67.66	−67.37
Na@6CT	−35.59	−35.10	−36.58	−33.41	−32.94	−34.53
Na$_3$O@6CT	−64.41	−59.67	−61.95	−60.90	−56.18	−58.54
K@6CT	−40.51	−39.83	−42.19	−39.34	−38.72	−41.11
K$_3$O@6CT	−71.19	−61.45	−60.82	−73.76	−64.29	−66.06

−71.86 and −70.34 kcal mol^{-1} at M05-2X/6-31G(d,p), M05-2X/6-31+G(d,p) and M05-2X/6-311+G(d,p) level of theory, respectively.

Similarly, in case of AA@6CT complexes, lithium doped complex also shows higher stability with the interaction energies of −41.07, −40.26 and −41.90 kcal mol^{-1} at 6-31G (d,p), 6-31+G(d,p) and 6-311+G(d,p) basis sets, respectively. Quite similar to M05-2X, Li and Li$_3$O doped complexes also exhibit higher stability at M06-2X with a small exception at 6-31G(d,p) basis set. The interaction energies of Li$_3$O@6CT complexes are −72.76, −67.66 and −67.37 kcal mol^{-1} while Li@6CT complex are −39.54, −38.85 and −40.44 kcal mol^{-1} at M06-2X/6-31G(d,p), /6-31+G(d,p) and /6-311+G(d,p), respectively. Owing to the smallest atomic size, the lithium atom interacts more closely to the 6CT which is further evident by the least interaction distance (I_d) among all SA@6CT and AA@6CT complexes. The interaction distances of Li$_3$O@6CT and Li@6CT complexes are 2.62 and 2.55 Å, respectively (see Table 2) which are least among all the other complexes.

The stability of the lithium-based complexes is followed by the potassium doped complexes. The high stability of K$_3$O@6CT complex can be explained by examining the geometry. Fig. 1 reveals that only a single K atom equally interacts with all the sulfur atoms of 6CT unlike Na doped complexes where interaction of sodium is with some sulfur atoms. The interaction distances (K···S) of K or K$_3$O and 6CT are 3.30 and 3.11 Å, respectively. The average interaction distances between sodium atom of Na and Na$_3$O with sulfur atoms of 6CT are 2.84 and 3.02 Å, respectively. The interaction energies of K$_3$O@6CT and K@6CT complexes are higher at all methods than Na$_3$O@6CT and Na@6CT complexes, respectively (see Table 1). It can be seen from the results, the basis set 6-31G(d,p) (without

polarization) overestimates the energy values while 6-31+G(d,p) basis set predicts higher accuracy in the results.

3.2 Electronic properties

Molecular orbital analysis is performed to examine and compare the variation of electronic parameters of 6CT upon complexation with alkali atoms and superalkalis. The energies of HOMO and LUMO orbitals and their differences (E_{H-L}) in eV are given in Table 2. The E_{H-L} of isolated 6CT is 5.02 eV where the energies of HOMO and LUMO are −6.43 and −0.24 eV, respectively. The E_{H-L} of 6CT decreases upon complexation due to the formation of new energy levels.[33] In comparison with alkali metals, the superalkalis doping widely reduces the H–L gaps which reflects the large availability of excess electrons in SA@6CT complexes. The E_{H-L} of 6CT is reduced to 3.15, 2.96 and 3.29 eV in Li$_3$O@6CT, Na$_3$O@6CT and K$_3$O@6CT complexes, respectively. On the other hand, the E_{H-L} of Li@6CT, Na@6CT and K@6CT complexes are 3.27, 3.14 and 2.93 eV, respectively. The decrease in the H–L gaps of complexes is due to the variation in the energies of HOMO and LUMO orbitals upon complexation with alkali metals and superalkalis. For instant, the LUMO energy of 6CT (−0.24 eV) reduces to −1.31, −1.00 and −1.48 eV on interaction with Li, Na, and K atoms, respectively. Similarly, the LUMO energies of Li$_3$O@6CT, Na$_3$O@6CT and K$_3$O@6CT complexes are shifted to −1.44, −1.54 and −1.24 eV, respectively. The decreasing trends of LUMO energies of AA@6CT and SA@6CT complexes are as follow; K > Li > Na and Na$_3$O > Li$_3$O > K$_3$O, respectively. Moreover, the trend of increasing energies of HOMO orbital for AA@6CT and SA@6CT complexes are; K > Na > Li and Na$_3$O > K$_3$O > Li$_3$O, respectively. The effects of K and Na$_3$O in H–L gaps of AA@6CT and SA@6CT

Table 2 Interaction parameters of optimized geometries of SA@6CT and AA@6CT complexes

Complexes	Sym	Int bond	Int distance (Å)	HOMO (eV)	LUMO (eV)	E_{H-L} (eV)	Q (e^-)
6CT	C_1	—	—	−6.43	−0.24	5.02	—
Li@6CT	C_1	Li···S	2.55	−4.58	−1.31	3.27	0.60
Li$_3$O@6CT	C_1	Li···S	2.62	−4.59	−1.44	3.15	1.69
Na@6CT	C_1	Na···S	2.84	−4.54	−1.00	3.14	0.76
Na$_3$O@6CT	C_1	Na···S	3.02	−4.50	−1.54	2.96	1.53
K@6CT	C_1	K···S	3.30	−4.01	−1.48	2.93	0.75
K$_3$O@6CT	C_1	K···S	3.11	−4.54	−1.24	3.29	0.91

complexes, respectively are more pronounced. Therefore, the K@6CT and Na$_3$O@6CT complexes show the lowest H–L gap among in their series. Furthermore, DOS spectra reveal (Fig. 3) that the generation of new HOMO/occupied energy levels on interaction plays pivotal role to lower the E_{H-L} gaps of complexes. It is clearly seen in Fig. 2 that the HOMO orbitals of the systems mainly reside near the doped alkali atoms or superalkalis, indicating the generation of new HOMO orbitals which are further responsible of producing excess electrons in the system. The DOS spectrum in Fig. 3 reveals that the occupied and virtual orbitals of isolated 6CT are located at −6.43 and −0.24 eV, respectively. Upon complexation with alkali atoms and superalkalis, the spin state has been changed from singlet (in 6CT) to doublet (in AA@6CT and SA@6Ct complexes) due to the involvement of unpaired electrons from doped metal atoms. Moreover, the occupied orbitals of the 6CT are shifted closer to the Fermi level on interaction. The occupied orbitals appear at −4.58, −4.54, −4.01 eV (light blue colour) in Li@6CT, Na@6CT and K@6CT complexes, respectively. However, the occupied orbitals peaks of Li$_3$O@6CT, Na$_3$O@6CT and K$_3$O@6CT complexes appear at −4.59, −4.50 and −4.54 eV, respectively. Moreover, the peaks (red colour) in the DOS spectrum of 6CT are also shifted toward Fermi level upon complexation with alkali and superalkalis (light brown peaks). From DOS analysis, it

can be concluded that the HOMO and LUMO energy gaps of AA@6CT and SA@6CT complexes decrease due to the shift or generation of new orbitals close to the Fermi level.

NBO analysis is performed to examine the charge transfer between 6CT and AA or SA. Expectedly, the charge transfer in SA@6CT complexes is higher than AA@6CT complexes due to the large electronic density on superalkalis. The NBO charge transferred (Q) in Li$_3$O@6CT, Na$_3$O@6CT and K$_3$O@6CT complexes is 1.69, 1.53 and 0.91e^-, respectively. Probably, some of the electronic density is shifted from alkali atoms toward the covalently bonded electronegative oxygen atom of superalkalis. This charge transfer increases with decreasing the electronegativity of alkali atoms from Li to Na. Due to the increasing charge transfer between the atoms of superalkalis, the charge transfer decreases between superalkalis and 6CT from Li$_3$O to Na$_3$O. On the other side, the amount of charge transfer increases upon increasing atomic number of alkali atoms. The amounts of charge transfer is 0.60, 0.76 and 0.75e^- in Li@6CT, Na@6CT and K@6CT complexes, respectively.

3.3 UV-vis analysis

It is postulated that NLO active material should be transparent in the interested region of EMR spectrum.[34] In order to find the
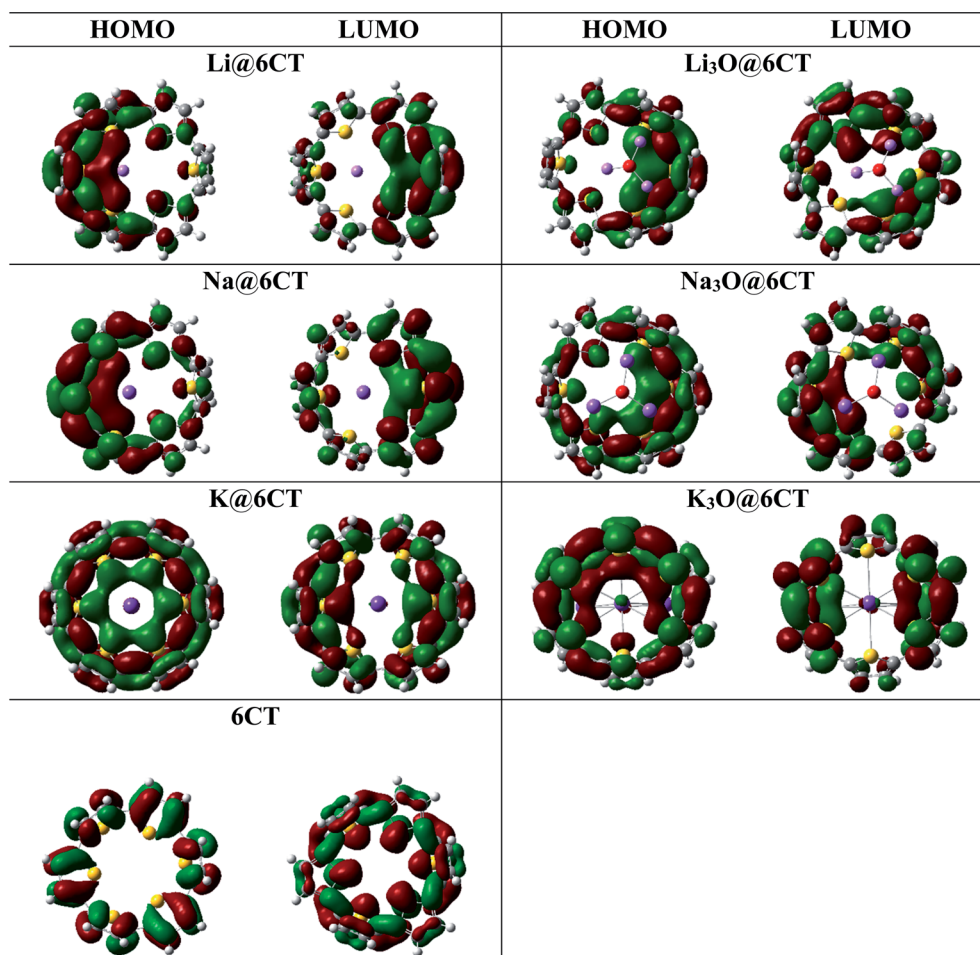
Fig. 2 HOMO and LUMO orbitals of 6CT, AA@6CT and SA@6CT complexes.

adsorption wavelength of 6CT before and after doping, the UV-vis analysis is performed at TD/M05-2X/6-31+G(d,p). It is cleared from the results (Table 3 & Fig. 4) that the maximum absorption of isolated 6CT appears at 328 nm. The absorption spectrum of 6CT splits into two red shifted peaks in visible region upon complexation especially with Li, Na, K and Li$_3$O. Firstly, the red

Fig. 3 DOS spectra of 6CT, AA@6CT and SA@6CT complexes.

Table 3 NLO parameters: dipole moment (μ_o), polarizability (α_o), first hyperpolarizability (β_o), projection of β on dipole moment vec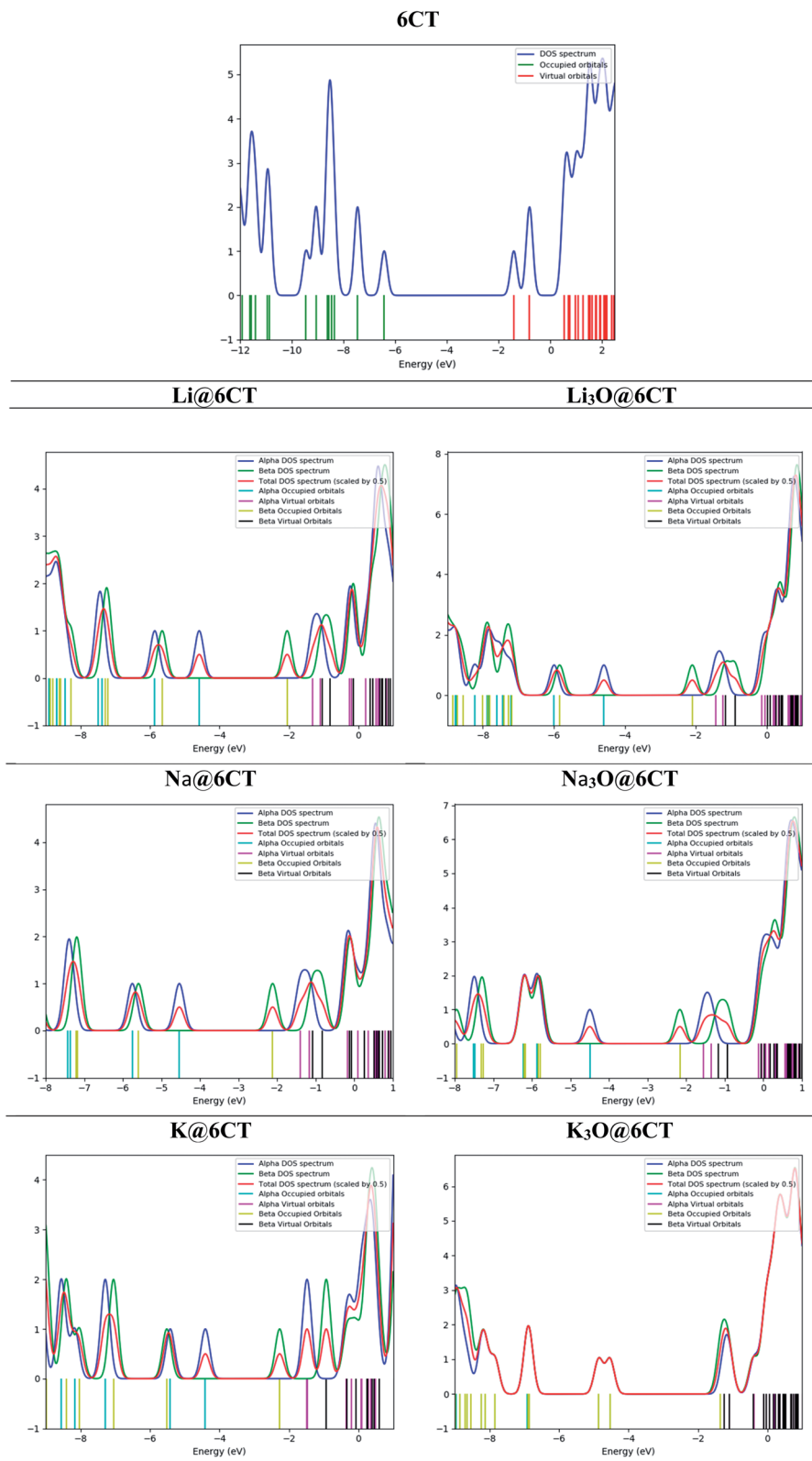tor (β_{vec}), hyper-Rayleigh (β_{HRS}), second hyperpolarizability (γ_o), crucial excitation energies (E_{ex}), change in dipole moment ($\Delta\mu$), vertical ionization energy (V_{IE}), maximum absorbance (λ_{max}) and oscillator strength (f_o) of isolated 6CT and AA@6CT & SA@6CT complexes

LC-BLYP

Complexes units	μ_o D	α_o au	β_o au	β_{vec} au	β_{HRS} au	γ_o au	ΔE_{ex} eV	$\Delta\mu$ D	V_{IE} eV	λ_{max} nm	f_o au
6CT	4.85	384.56	2×10^2	—	—	—	0.85	1.19	6.96	328	0.49
Li@6CT	6.00	528.90	3×10^4	1.5×10^4	1.5×10^4	2.0×10^6	3.10	1.76	5.02	424	0.38
Li$_3$O@6CT	6.50	529.20	2×10^4	9.8×10^3	1.1×10^4	1.7×10^6	3.10	1.38	5.03	425	0.28
Na@6CT	6.93	562.53	4×10^4	2.3×10^4	2.4×10^4	4.1×10^6	3.06	2.31	4.98	443	0.21
Na$_3$O@6CT	6.89	581.13	5×10^4	2.5×10^4	2.7×10^4	2.6×10^6	1.66	6.19	4.94	883	0.09
K@6CT	7.27	375.62	5×10^3	3.9×10^3	2.3×10^3	5.6×10^6	2.96	1.34	4.92	448	0.71
K$_3$O@6CT	13.17	553.15	3×10^3	2.5×10^3	1.3×10^3	3.6×10^5	2.39	2.95	6.33	809	0.04

shift in the UV-vis spectra of AA@6CT and SA@6CT complexes articulates the increasing π–π^* transitions. Results reveal that all the reported materials are transparent in ultraviolet region. However, the Na$_3$O@6CT and K$_3$O@6CT complexes show good transparency in both ultraviolet and visible regions due to the absence of peak maxima between 200 to 800 nm. In comparison, Na$_3$O@6CT and K$_3$O@6CT complexes indicate adequate transparency for laser applications in both UV and vis regions.

4 Nonlinear optical properties

4.1 Static NLO responses

The values of dipole moment (μ_o) and polarizabilities (α_o) of isolated and complexed 6CT are given in Table 3. The dipole moment of 6CT is 4.85 D due to its C_1 symmetry (Table 2). However, the dipole moment of 6CT increases upon complexation with alkali metals and superalkalis due to the distortion of symmetry. The dipole moments are ranging from 6.00 to 7.27 D and 6.50 to 13.17 D in AA@6CT and SA@6CT series, respectively. Similarly, the static polarizabilities of SA@6CT complexes are higher than AA@6CT complexes due to the greater electronic contribution of superalkalis. The polarizabilities of Na@6CT and Na$_3$O@6CT complexes are the highest among all complexes which is well consistent with the hyperpolarizabilities (*vide infra*). The α_o of AA@6CT complexes is ranging from 375.62 au (K@6CT) to 562.53 au (Na@6CT) whereas, these values range from 528.90 to 553.15 au for SA@6CT complexes.

The static hyperpolarizabilities of the designed complexes have been computed to explore their NLO responses and the results are listed in Table 3 & Fig. 5. The static hyperpolarizability (β_o) of isolated 6CT is 2×10^4 au. The complexation of alkali metal and superalkalis remarkably boost the β_o of 6CT to lie in the range of 2×10^4–5×10^4 au. Surprisingly, the NLO responses of Li and K doped 6CT is higher than their corresponding superalkalis complexes. The lower NLO responses of Li$_3$O@6CT and K$_3$O@6CT complexes are probably due to the higher vertical ionization energy (V_{IE}) values[33] which reflects the removal of electron is difficult from these systems. On the hand, Na$_3$O@6CT complex exhibits lower V_{IE} (4.94 eV) than corresponding Na@6CT complex, therefore, the β_o of former is far higher than the later complexes. Furthermore,

β_o results reveal that the Na$_3$O@6CT complex is highly NLO active among other designed complexes.

To support these findings, the projection of static hyperpolarizability on the dipole moment vector (β_{vec}) is also computed. The trend of β_{vec} is exactly consistent to the β_o of complexes which reveals that Na$_3$O@6CT complex is highly NLO sensitive while K$_3$O@6CT complex shows least sensitivity. These findings are well comparable to the above-mentioned electronic parameters especially HOMO–LUMO gap and NBO charge transfer analysis. The hyperpolarizability of superalkalis doped complex agrees well with the previously reported similar superalkalis doped cyclic conjugated ring systems. In our previous study, we have reported that the β_o of superalkalis doped cyclic oligofuran systems was appreciably high and ranges from 1×10^4 to 2×10^4 au especially in Li$_3$O doped complexes.[27] In another similar study, the reported β_o of lithium doped cyclic conjugated ring system was 7.3×10^3 au[33] and 3×10^4 au.[34] In this study, we found that the NLO responses of alkali and superalkalis doped 6CT complexes have shown good agreement with the previously reported similar systems.[35,36]

Two level model is performed to interpret the effects of change in dipole moment ($\Delta\mu$), oscillator strength (f_o) and crucial excited
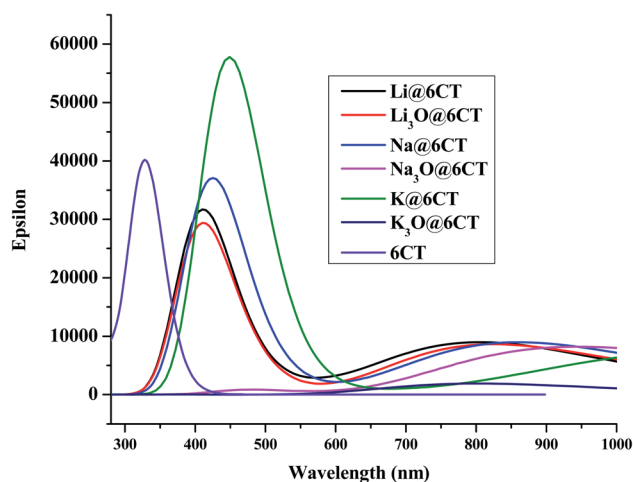

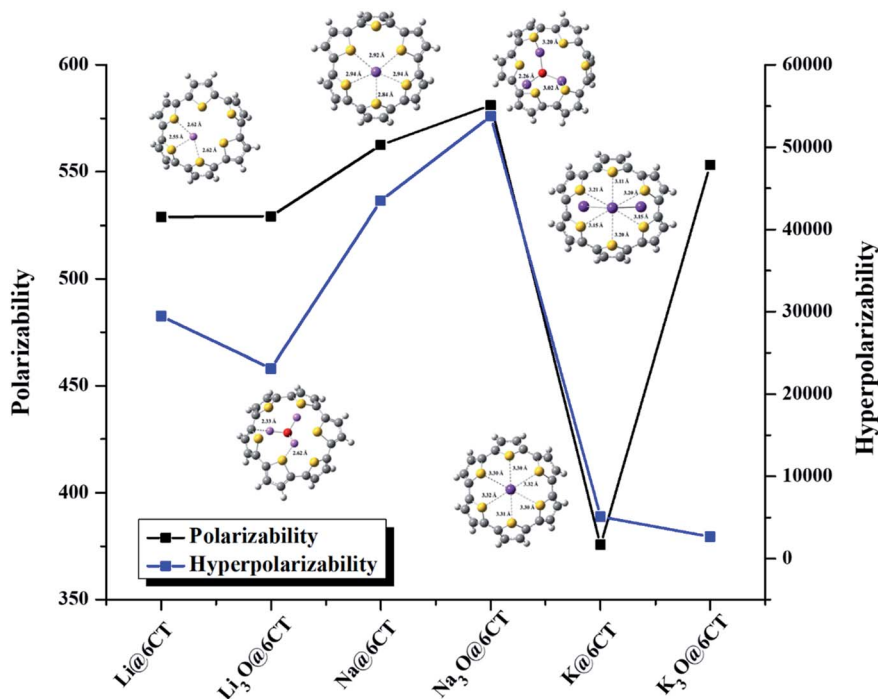**Fig. 4** UV-vis spectra of 6CT, AA@6CT and SA@6CT complexes.

Fig. 5 Graphical representation of polarizability and hyperpolarizability of AA@6CT and SA@6CT complexes.

energy (ΔE_{ex}) on the hyperpolarizability of complexes. The two-level model can be defined by the expression below;[37]

$$\beta_o \propto f_o \times \Delta\mu/\Delta E_{ex}^3$$

Based on the above equation, the β_o increases with increasing values of oscillator strength or the change in dipole moment. On the other side, the value of β_o is lower if a complex exhibits high crucial excited energy. The results illustrate that the Na$_3$O@6CT complex shows the highest β_o which might be due to the largest value of $\Delta\mu$ (6.19 D). The lowest value of crucial excited energy (1.66 eV) is also contributing to the higher hyperpolarizability of Na$_3$O@6CT complex. Similarly, the smallest oscillator strength (f_o) (0.04 au) of K$_3$O@6CT complex plays a vital role of exhibiting small NLO response.

The static second hyperpolarizability (γ_o) values are also estimated and the results revealed that γ_o values have trend similar to that of β_o but the γ_o values are significantly larger. The γ_o values of the designed complexes are in the range of 3.6×10^5 to 5.6×10^6 au. According to previous results,[38] the giant NLO response in the alkali and superalkali doped cyclic thiophene may be caused by the excess electrons of doped alkali/superalkali.

Due to the lack of experimental results, the hyperpolarizability of complexes are also calculated at M05-2X and M06-2X with different basis sets including 6-31G(d,p), 6-31+G(d,p) and 6-311+G(d,p) (Table 4). The trend of hyperpolarizability of AA@6CT and SA@6CT complexes at Minnesota functional is quite comparable with LC-BLYP. Like LC-BLYP, the β_o of Na$_3$O@6CT complex is the highest in all the cases with little exception at 6-31+G(d,p) and 6-311+G(d,p) basis sets.

The β_o of Na@6CT and Na$_3$O@6CT are 2.3×10^4 and 2.9×10^4 au, respectively at M05-2X/6-31+G(d,p) level of theory, the highest compared to other AA@6CT and SA@6CT complexes. At M06-2X, the β_o values of Na@6CT and Na$_3$O@6CT complexes are 2.2×10^4 and 2.6×10^4 au which is quite consistent with the results of competing M05-2X method. Though the trend is same with LC-BLYP but the values of β_o for complexes are appreciably lower at Minnesota functionals. Moreover, LC-BLYP is a full range separated functional with 1.00 fraction for nonlocal exchange at asymptotic distance.[39,40] Therefore, the nonlinear optical results of material are more reliable at LC-BLYP[15] thus, the dynamic hyperpolarizability has been calculated at widely accepted LC-BLYP.

4.2 Dynamic NLO responses

The dynamic first hyperpolarizability coefficients i.e. electro-optic Pockel's effect (EOPE) with $\beta(-\omega, \omega, 0)$ and the second-harmonic generation (SHG) with $\beta(-2\omega, \omega, \omega)$ of the designed complexes are calculated and the values are given in Table 5. The frequency dispersion analysis was performed with the wavelengths of 532 nm (0.0856 au) and 1064 nm (0.0428 au) in order to provide a frequency dependent NLO response at the routinely utilized Nd:YAG laser frequencies. The calculated results revealed that the first hyperpolarizability $\beta(\omega)$ coefficients are dependent on the wavelengths. One can see that the static first hyperpolarizability of the designed complexes are in the range of 3×10^3 to 5×10^4 au while the frequency dependent response are largely enhanced. The EOPE values at 1064 nm are in the range of 3.1×10^3 to 1.9×10^6 au. The EOPE values are further enhanced to the range of 3.6×10^4 to 7.2×10^7 au at shorter wavelength of 532 nm. This indicates that

Table 4 Hyperpolarizability (β_o in au) of SA@6CT and AA@6CT complexes at M052X and M062X methods

Complexes	M052X			M062X		
	6-31G (d,p)	6-31+G (d,p)	6-311+G (d,p)	6-31G (d,p)	6-31+G (d,p)	6-311+G (d,p)
6CT	7.0×10^1	2.1×10^2	2.4×10^2	6.6×10^0	2.3×10^2	2.2×10^2
Li@6CT	1.6×10^4	1.8×10^2	1.8×10^4	1.6×10^4	1.8×10^4	1.8×10^4
Li$_3$O@6CT	1.6×10^4	1.8×10^4	1.9×10^4	1.6×10^4	1.9×10^4	1.9×10^4
Na@6CT	2.0×10^4	2.3×10^4	3.5×10^3	1.9×10^4	2.2×10^4	2.1×10^4
Na$_3$O@6CT	2.6×10^4	2.9×10^4	3.1×10^4	1.1×10^5	2.6×10^4	2.5×10^4
K@6CT	3.0×10^2	3.8×10^2	4.6×10^2	4.1×10^2	1.9×10^2	2.6×10^2
K$_3$O@6CT	6.1×10^4	5.9×10^3	2.5×10^3	4.0×10^4	3.3×10^3	9.7×10^3

Table 5 Estimated values of $\beta(-\omega, \omega, 0)$, $\beta(-2\omega, \omega, \omega)$, $\gamma(-\omega, \omega, 0, 0)$, $\gamma(-2\omega, \omega, \omega, 0)$, γ^{DFWM}, and n_2 (cm^2 W^{-1}) in au

Parameters	Frequency ω	Li@6CT	Li$_3$O@6CT	Na@6CT	Na$_3$O@6CT	K@6CT	K$_3$O@6CT
$\beta(-\omega, \omega, 0)$	1064 nm	4.4×10^5	1.7×10^5	9.8×10^4	1.9×10^6	3.1×10^3	5.6×10^3
	532 nm	4.8×10^4	3.6×10^4	2.7×10^5	7.2×10^7	8.2×10^4	8.8×10^4
$\beta(-2\omega, \omega, \omega)$	1064 nm	7.7×10^5	2.7×10^5	5.6×10^5	2.0×10^8	8.8×10^3	1.6×10^5
	532 nm	9.2×10^4	2.5×10^4	5.8×10^4	2.2×10^7	4.9×10^4	1.7×10^5
$\gamma(-\omega, \omega, 0,0)$	1064 nm	5.1×10^7	7.8×10^6	1.4×10^8	1.5×10^9	8.1×10^5	1.0×10^6
	532 nm	4.0×10^6	4.6×10^6	3.5×10^7	3.7×10^{10}	2.2×10^8	4.4×10^7
$\gamma(-2\omega, \omega, \omega, 0)$	1064 nm	2.1×10^8	7.4×10^7	9.4×10^7	1.3×10^{11}	5.5×10^6	1.4×10^7
	532 nm	1.5×10^7	1.0×10^7	3.2×10^6	2.9×10^{10}	2.4×10^7	6.7×10^8
γ^{DFWM}	1064 nm	1.2×10^8	3.2×10^7	1.7×10^8	4.6×10^{10}	7.9×10^5	5.7×10^6
	532 nm	8.2×10^6	7.4×10^6	3.5×10^7	4.6×10^{10}	2.3×10^8	2.7×10^8
n_2 (cm^2 W^{-1})	1064 nm	1.0×10^{-14}	2.7×10^{-15}	1.4×10^{-14}	3.8×10^{-12}	6.6×10^{-17}	4.7×10^{-16}
	532 nm	6.9×10^{-16}	6.2×10^{-16}	2.9×10^{-15}	3.8×10^{-12}	1.9×10^{-14}	2.2×10^{-14}

EOPE values are more susceptible to shorter wavelength (532 nm). The second-harmonic generation (SHG) coefficient $\beta(-2\omega, \omega, \omega)$ values of the designed complexes lie in the range of 8.8×10^3 to 2.0×10^8 au at 1064 nm and decreases to the range of 2.5×10^4 to 2.2×10^7 au which indicates that the resonant enhancement for SHG process takes place at higher wavelength (1064 nm). Overall SHG process has stronger NLO response than EOPE at wavelength of 1064 nm for all designed complexes however, shorter wavelength 532 nm induces slightly stronger EOPE response than SHG process for Li$_3$O@6CT, Na@6CT, Na$_3$O@6CT, and K@6CT complexes.

The dynamic second hyperpolarizability coefficients including dc-Kerr effect $\gamma(-\omega, \omega, 0, 0)$ and the electric field-induced second harmonic generation (ESHG) $\gamma(-2\omega, \omega, \omega, 0)$ are also computed and the results are listed in the Table 5. Like dynamic first hyperpolarizability analysis, the frequency dispersion analysis was performed with the same wavelengths of 532 nm (0.0856 au) and 1064 nm (0.0428 au). From Table 5, one can see that the designed complexes have remarkably large dc-Kerr effect (up to 3.7×10^{10} au) and ESHG (up to 1.3×10^{11} au). The largest dc-Kerr effect and ESHG response was shown by Na$_3$O@6CT complex. From static, dc-Kerr and ESHG second hyperpolarizability coefficients, degenerate four-wave mixing (DFWM), $\gamma^{DFWM}(\omega) = \gamma(-\omega, \omega, -\omega, \omega)$ was calculated using the following equation:[41]

$$\gamma^{DFWM}(-\omega, \omega, -\omega, \omega) \approx (1/3)\gamma(-2\omega, \omega, \omega, 0) + \gamma(-\omega, \omega, 0, 0) - (1/3)\gamma(0, 0, 0, 0)$$

Then from DFWM values we can evaluate the quadratic nonlinear refractive index (n_2) using the following equation:[42]

$$n_2 \text{ (cm}^2 \text{ W}^{-1}) = 8.28 \times 10^{-23}\gamma^{DFWM} \text{ (au)}$$

The values of quadratic nonlinear refractive index (n_2) are significantly large for all complexes. At wavelength of 1064 nm, the n_2 values ranges from 6.6×10^{-17} to 3.8×10^{-12} au and at 532 nm, the n_2 values are in the range of 6.9×10^{-16} to 3.8×10^{-12} au. The n_2 values as a function of wavelength confirm that the amplitude of the second order nonlinear optical response is expected to vary with changes in wavelength as well as different alkali metal.

5 Conclusions

In this research, a series of complexes have been designed by doping alkali metal atoms (Li, Na and K) and superalkalis (Li$_3$O, Na$_3$O & K$_3$O) for nonlinear optical applications. The interaction energies at M05-2X and M06-2X with 6-31G(d,p), 6-31+G(d,p) and 6-311+G(d,p) basis sets reveal that the reported complexes are thermodynamically stable. In comparison, the interaction

stabilities of superalkalis@6CT complexes are far higher than alkali atoms@6CT complexes. Furthermore, the doping of alkali metals and their corresponding superalkalis leads to remarkably high NLO responses. Among all the complexes, $Na_3O@6CT$ complex exhibits highest NLO response. The static hyperpolarizability of $Na_3O@6CT$ complex is 5×10^4 au along with pronounced β_{vec} value (2.5×10^4 au) and significantly large quadratic nonlinear optical response (3.8×10^{-12} au). The electronic properties provide evidence of high NLO response of $Na_3O@6CT$ complex. For example, $Na_3O@6CT$ complex shows an appreciable amount of NBO charge transfer ($1.53e^-$) along with the considerably low E_{H-L} gap (2.96 eV). The absorption spectrum also illustrates the ultra-high transparency of $Na_3O@6CT$ complex in UV-vis region. Finally, the improved second-harmonic generation, electro-optic Pockel's effect and nonlinear refractive index of our alkali/superalkali doped 6CT complexes open new prospective for the designing of new NLO material, especially $Na_3O@6CT$, for opto-electronic applications.

Conflicts of interest

There are no conflicts to declare.

Acknowledgements

References

1 D. F. Eaton, *Science*, 1991, **253**, 281–287.
2 W.-D. Cheng, K.-H. Xiang, R. Pandey and U. C. Pernisz, *J. Phys. Chem. B*, 2000, **104**, 6737–6742.
3 V. M. Geskin, C. Lambert and J.-L. Brédas, *J. Am. Chem. Soc.*, 2003, **125**, 15651–15658.
4 M. Ichida, T. Sohda and A. Nakamura, *J. Phys. Chem. B*, 2000, **104**, 7082–7084.
5 B. Kirtman, B. Champagne and D. M. Bishop, *J. Am. Chem. Soc.*, 2000, **122**, 8007–8012.
6 S. Muhammad, H.-L. Xu, R.-L. Zhong, Z.-M. Su, A. G. Al-Sehemi and A. Irfan, *J. Mater. Chem. C*, 2013, **1**, 5439.
7 C.-L. Wu, Y.-H. Lin, S.-P. Su, B.-J. Huang, C.-T. Tsai, H.-Y. Wang, Y.-C. Chi, C.-I. Wu and G.-R. Lin, *ACS Photonics*, 2015, **2**, 1141–1154.
8 W. Chen, Z.-R. Li, D. Wu, Y. Li, C.-C. Sun and F. L. Gu, *J. Am. Chem. Soc.*, 2005, **127**, 10977–10981.
9 R.-L. Zhong, H.-L. Xu, S.-L. Sun, Y.-Q. Qiu and Z.-M. Su, *Chem.–Eur. J.*, 2012, **18**, 11350–11355.
10 W. Chen, Z.-R. Li, D. Wu, R.-Y. Li and C.-C. Sun, *J. Phys. Chem. B*, 2005, **109**, 601–608.
11 Y.-Q. Jing, Z.-R. Li, D. Wu, Y. Li, B.-Q. Wang, F. L. Gu and Y. Aoki, *ChemPhysChem*, 2006, **7**, 1759–1763.
12 A. S. Ichimura, J. L. Dye, M. A. Camblor and L. A. Villaescusa, *J. Am. Chem. Soc.*, 2002, **124**, 1170–1171.
13 B. Champagne, M. Spassova, J.-B. Jadin and B. Kirtman, *J. Chem. Phys.*, 2002, **116**, 3935–3946.
14 M. Spassova, B. Champagne and B. Kirtman, *Chem. Phys. Lett.*, 2005, **412**, 217–222.
15 S. Munsif, Maria, S. Khan, A. Ali, M. A. Gilani, J. Iqbal, R. Ludwig and K. Ayub, *J. Mol. Liq.*, 2018, **271**, 51–64.
16 Maria, J. Iqbal and K. Ayub, *J. Alloys Compd.*, 2016, **687**, 976–983.
17 Maria, J. Iqbal, R. Ludwig and K. Ayub, *Mater. Res. Bull.*, 2017, **92**, 113–122.
18 G. L. Gutsev and A. I. Boldyrev, *Chem. Phys. Lett.*, 1982, **92**, 262–266.
19 F. Ullah, N. Kosar, K. Ayub and T. Mahmood, *Appl. Surf. Sci.*, 2019, **483**, 1118–1128.
20 F. Ullah, N. Kosar, K. Ayub, M. A. Gilani and T. Mahmood, *New J. Chem.*, 2019, **43**, 5727–5736.
21 F. Ullah, N. Kosar, M. N. Arshad, M. A. Gilani, K. Ayub and T. Mahmood, *Opt. Laser Technol.*, 2020, **122**, 105855.
22 C. Hu, Z. Chen, H. Xiao, Z. Zhen, X. Liu and S. Bo, *J. Mater. Chem. C*, 2017, **5**, 5111–5118.
23 F. Liu, Y. Yang, S. Cong, H. Wang, M. Zhang, S. Bo, J. Liu, Z. Zhen, X. Liu and L. Qiu, *RSC Adv.*, 2014, **4**, 52991–52999.
24 H. Sajid, F. Ullah, M. Yar, K. Ayub and T. Mahmood, *New J. Chem.*, 2020, **44**, 16358–16369.
25 K. Shehzadi, K. Ayub and T. Mahmood, *Appl. Surf. Sci.*, 2019, **492**, 255–263.
26 N. Kosar, K. Shehzadi, K. Ayub and T. Mahmood, *J. Mol. Graphics Modell.*, 2020, **97**, 107573.
27 H. Sajid, K. Ayub and T. Mahmood, *New J. Chem.*, 2020, **44**, 2609–2618.
28 M. J. Frisch, G. W. Trucks, H. B. Schlegel, G. E. Scuseria, M. A. Robb, J. R. Cheeseman, G. Scalmani, V. Barone, B. Mennucci, G. A. Petersson, H. Nakatsuji, M. Caricato, X. Li, H. P. Hratchian, A. F. Izmaylov, J. Bloino, G. Zheng, J. L. Sonnenberg, M. Hada, M. Ehara, K. Toyota, R. Fukuda, J. Hasegawa, M. Ishida, T. Nakajima, Y. Honda, O. Kitao, H. Nakai, T. Vreven, J. A. Montgomery Jr, J. E. Peralta, F. Ogliaro, M. J. Bearpark, J. Heyd, E. N. Brothers, K. N. Kudin, V. N. Staroverov, R. Kobayashi, J. Normand, K. Raghavachari, A. P. Rendell, J. C. Burant, S. S. Iyengar, J. Tomasi, M. Cossi, N. Rega, N. J. Millam, M. Klene, J. E. Knox, J. B. Cross, V. Bakken, C. Adamo, J. Jaramillo, R. Gomperts, R. E. Stratmann, O. Yazyev, A. J. Austin, R. Cammi, C. Pomelli, J. W. Ochterski, R. L. Martin, K. Morokuma, V. G. Zakrzewski, G. A. Voth, P. Salvador, J. J. Dannenberg, S. Dapprich, A. D. Daniels, Ö. Farkas, J. B. Foresman, J. V. Ortiz, J. Cioslowski and D. J. Fox, *Gaussian 09, Rev. C. 01*, Wallingford CT, 2009.
29 N. M. O'boyle, A. L. Tenderholt and K. M. Langner, *J. Comput. Chem.*, 2008, **29**, 839–845.
30 A. Shokuhi and K. Ayub, *Mater. Res. Bull.*, 2018, **97**, 399–404.
31 F. L. Gu, Y. Aoki, M. Springborg and B. Kirtman, *Calculations on nonlinear optical properties for large systems*, 2015, pp. 67–83.
32 T. Lu and F. Chen, *J. Comput. Chem.*, 2012, **33**, 580–592.
33 F. Ullah, K. Ayub and T. Mahmood, *New J. Chem.*, 2020, **44**, 9822–9829.

34 W.-M. Sun, C.-Y. Chen, C.-Y. Li, D. Wu, J. Kang, Y. Li and Z.-R. Li, *ChemPhysChem*, 2018, **19**, 2518–2524.

35 R.-L. Zhong, H.-L. Xu, Z.-R. Li and Z.-M. Su, *J. Phys. Chem. Lett.*, 2015, **6**, 612–619.

36 W.-M. Sun, L.-T. Fan, Y. Li, J.-Y. Liu, D. Wu and Z.-R. Li, *Inorg. Chem.*, 2014, **53**, 6170–6178.

37 J. L. Oudar and D. S. Chemla, *J. Chem. Phys.*, 1976, **66**, 2664–2668.

38 X. Li, Y. Zhang and J. Lu, *Appl. Surf. Sci.*, 2020, **512**, 145544.

39 M. Maria, J. Iqbal and K. Ayub, *RSC Adv.*, 2016, **6**, 94228–94235.

40 M. B. Oviedo, N. V. Ilawe and B. M. Wong, *J. Chem. Theory Comput.*, 2016, **12**, 3593–3602.

41 M. Tarazkar, D. A. Romanov and R. J. Levis, *J. Chem. Phys.*, 2014, **140**, 214316.

42 C. Brée, A. Demircan and G. Steinmeyer, *IEEE J. Quantum Electron.*, 2010, **46**, 433–437.